Chemical Physics 469-470 (2016) 25–30

Contents lists available at ScienceDirect

Chemical Physics

journal homepage: www.elsevier.com/locate/chemphys

Ultrafast Exciton Dynamics in $Cd_xHg_{(1-x)}Te$ alloy Quantum Dots

Marina A. Leontiadou [a,*], Ali Al-Otaify [a,b], Stephen V. Kershaw [c], Olga Zhovtiuk [c], Sergii Kalytchuk [c], Derrick Mott [d], Shinya Maenosono [d], Andrey L. Rogach [c], David J. Binks [a]

[a] School of Physics and Astronomy and Photon Science Institute, University of Manchester, Manchester M13 9PL, UK
[b] Department of Physics, College of Science, Qassim University, Saudi Arabia
[c] Department of Physics and Material Science, City University of Hong Kong, Hong Kong Special Administrative Region
[d] School of Materials Science, Japan Advanced Institute of Science and Technology, 1-1 Asahida, Nomi, Ishikawa 923-1292, Japan

ARTICLE INFO

Article history:
Received 27 November 2015
In final form 2 February 2016
Available online 24 February 2016

Keywords:
Multiple exciton generation
Femtosecond transient absorption spectroscopy
CdHgTe alloy quantum dot

ABSTRACT

Ultrafast transient absorption spectroscopy is used to investigate sub-nanosecond exciton dynamics in $Cd_xHg_{(1-x)}Te$ alloy colloidal quantum dots. A bleach was observed at the band gap due to state-filling, the mono-exponential decay of which had a characteristic lifetime of 91 ± 1 ps and was attributed to biexciton recombination; no evidence of surface-related trapping was observed. The rise time of the bleach, which is determined by the rate at which hot electrons cool to the band-edge, ranged between 1 and 5 ps depending on the pump photon energy. Measuring the magnitude of the bleach decay for different pump fluences and wavelengths allowed the quantum yield of multiple exciton generation to be determined, and was 115 ± 1% for pump photons with energy equivalent to 2.6 times the band gap.

1. Introduction

Colloidal quantum dots (QDs) have potential use in a number of applications, including in photovoltaic cells [1–3], displays and lighting [4], and photorefractive devices [5]. For solar cells, size-control of these materials allows the band gap to be tuned so that it is optimum for exploitation of the solar spectrum [6,7]. Mercury telluride (HgTe) is particularly well-suited for use as the photo-absorbing species in solar cells because its almost zero bulk band gap allows HgTe QDs to be size-tuned throughout the near-infrared region [2]. This type of QD benefits from additional flexibility because the band gap of QDs can also be composition-tuned via alloying with cadmium to produce $Cd_xHg_{(1-x)}Te$ [8]. Furthermore, the band gap and the valence band split-off energies come into resonance at a certain composition value [9] which can lower the energy required for carrier multiplication, also known as multiple exciton generation (MEG) [10–13]. Hence, with the combined effect of size- and composition-tuning, this resonance could be moved towards the optimum energy for exploitation of the solar spectrum [9]. Thus $Cd_xHg_{(1-x)}Te$ QDs with split-off energy difference ~1 eV are of particular interest as the photo-absorbing species for the next generation solar cells.

The utility of QDs in solar cells often depends on the dynamics of the photo-generated excitons on a sub-nanosecond time-scale. In particular, the rate of exciton recombination will determine the fraction of photo-generated charges that can be extracted to produce the output of a photovoltaic cell. Surface states produced by dangling bonds are known to enable a non-radiative recombination pathway that traps band-edge charges on a picosecond time-scale [14–16]. These surface states can also trap hot charges, introducing an additional cooling pathway and thus increasing the overall cooling rate [17]. This influences the quantum yield (QY) of photo-generated charges because it competes with MEG, which uses the energy of an absorbed photon in excess of the band gap to form additional electron–hole pairs [18]. MEG has been predicted to be efficient in $Cd_xHg_{(1-x)}Te$ QDs because impact ionization, the corresponding effect in bulk materials, is significant in CdHgTe avalanche photodiodes [19]. The additional excitons produced by MEG can only contribute to photocurrent, and thus improve the efficiency of solar cells based on QDs [20], if charge extraction can be achieved within the lifetime of the resulting multiexcitons, which also occurs on an ultrafast time-scale.

The sub-nanosecond exciton dynamics of HgTe QDs have been recently studied in detail using ultrafast transient absorption spectroscopy [21]. In contrast, only initial results have been reported for $Cd_xHg_{(1-x)}Te$ QDs to date [9], using an ultrafast transient grating (TG) technique. An increased TG component was reported for a pump wavelength of 290 nm and was attributed to the additional biexcitons formed by MEG. However, whilst the decay time constant, τ_{decay}, for pumping above the MEG threshold was found, the TG method did not allow the recovery of τ_{decay} for pumping

* Corresponding author.
E-mail address: marina.leontiadou@manchester.ac.uk (M.A. Leontiadou).

http://dx.doi.org/10.1016/j.chemphys.2016.02.003
0301-0104/

below the MEG threshold. This prevented the confirmation that the TG observed above and below the MEG threshold was decaying at the same characteristic rate, and hence attributable due to biexciton recombination in both cases. Moreover, the potential effects of surface-trapping on the TG were not investigated and so their influence on the reported *QY* values cannot yet be excluded. In this work, ultrafast transient absorption (UTA) spectroscopy is used to further study the exciton dynamics in $Cd_xHg_{(1-x)}Te$ QDs, allowing a comparison of decay lifetimes above and below MEG threshold and thus confirmation that it is indeed MEG producing the observed differences in response. The rise-time of the UTA signal is also investigated enabling the electron cooling time to be determined for different pump wavelengths. The possibility of sub-nanosecond surface trapping is also investigated allowing the enhanced response at the shortest pump wavelengths to be more confidently attributed to MEG. Finally, the MEG *QY* is determined with a significantly improved accuracy and compared to the previous result.

2. Experimental Method

2.1. Sample Preparation

$Cd_xHg_{(1-x)}Te$ alloy QDs were produced from CdTe QDs by an ion exchange method, which was described in detail in a previous report [9] and so is only outlined here. The CdTe QDs, in aqueous solution and stabilized with thioglycerol, were synthesized using the one-pot method reported by Wu et al. [22]. These were continually converted into CdHgTe QDs by mixing with aliquots of mercury perchlorate solution, $Hg(ClO_4)_2{\cdot}2.5H_2O$ stabilized in alkaline solution with a small amount of additional ligand. The resulting CdHgTe alloy QDs were transferred into an organic solution by exchanging the thioglycerol for dodecanthiol, with the final product being $Cd_xHg_{(1-x)}Te$ QDs in tetrachloroethylene solvent (TCE). Transmission electron microscope image (see Fig. S1 in SI) shows that the QDs produced are 4.5 ± 0.5 nm in diameter. For optical characterization the samples were placed in 10 mm thick quartz cuvettes and diluted using TCE to obtain an absorbance at the band edge of between 0.2 and 0.5.

2.2. Spectroscopic Techniques

The photoluminescence (PL) and steady-state absorption spectra were measured using a Horiba Jobin Yvon Fluorolog model iHR(FL3-22) spectrofluorometer and a Perkin Elmer Lambda 1050 UV/Vis/NIR spectrometer, respectively.

The ultrafast transient absorption experiments were performed with the use of a mode-locked Ti:sapphire laser oscillator (Spectra-Physics Tsunami) and amplifier (Spectra Physics SpitfirePro) system, producing 100 fs, 1 mJ pulses at a wavelength of 800 nm and at a repetition rate of 1 kHz. A tunable pump beam was generated using 95% of the amplifier output, which was passed through an optical parametric amplifier (Light Conversion, TOPAS) with subsequent harmonic generator, before reaching the sample. At the sample, the pump beam had a diameter of 3 mm and a fluence up to 20 $\mu J/cm^2$. An optical chopper was used to modulate the pump at 500 Hz. The remainder of the amplifier output was used to produce the probe beam; it was directed, via a 200 mm long delay stage (Newport ILS), to a 2 mm thick sapphire crystal in order to generate the white light continuum. The probe was split into sample and reference beams; the sample beam was focussed to 1 mm diameter, whilst the reference beam bypassed the sample. Both beams were directed into a monochromator (Acton Research, SpectraPro 2500i) and detected by two silicon photodiodes. The signal amplitude was recorded with the use of a lock-in amplifier (Stanford Research Systems, SR830) synchronized to the optical chopper. All samples were stirred by a magnetic stirrer (Thermo Scientific, Variomag Mini) at ~1000 rpm throughout the experiment, unless otherwise stated. More details on the experimental set-up can be found elsewhere [23,24].

3. Results

3.1. Spectroscopic Characterization

Figure 1 shows the absorption (solid line) and PL (dashed line) spectra of the $Cd_xHg_{(1-x)}Te$ alloy QDs sample. The PL spectrum has a peak centred at 1043 nm with a FWHM of about 150 nm. In comparison, the absorption spectrum shows a broad shoulder, blue-shifted from the PL peak by approximately 130 nm, at about 920 nm, with a weak tail extending as far as the PL peak. These spectra are very similar to those observed for HgTe QDs, the forms of which were explained using detailed electronic structure modelling [21]. These calculations showed the PL peak corresponded to the conduction band minimum (CBM) to valance band maximum (VBM) transition. However, the same calculations also showed that the VBM-to-CBM absorbing transition is very weak compared to the transition from the VBM to the CBM-1 state. The absorption shoulder thus corresponds to this strong transition at higher energy, with a contribution from deeper in the valance band to the CBM also possible, and it is the weak tail extending to the PL peak that is produced by the lower energy VBM-to-CBM transition. We attribute the almost identical spectra observed here for CdHgTe QDs to the same cause. The position of the absorption edge is well-suited to the exploitation of the solar spectrum by a photovoltaic cell utilizing MEG [12]. As described in previous work [9], the composition of QDs of known diameter can be estimated from the position of the absorption edge. In this case this process yielded a value of $x = 0.5$.

Figure 2 shows the pump-induced intensity change spectrum for the QD sample for pumping at a wavelength of 500 nm and fluence of 16 $\mu J/cm^2$ obtained at the time corresponding to the peak signal (occurring at ~4 ps after the arrival of the pump pulse for this pump wavelength); for comparison, the corresponding spectra obtained for the TCE and under the same pumping conditions is also shown. The spectrum for the QDs comprises two overlapping peaks centred at approximately 920 nm and 1050 nm. In contrast, the spectrum for the TCE is featureless except for a sharp peak at the exactly half the pump wavelength, which is attributed to pump light scattered by the sample into the spectrometer and

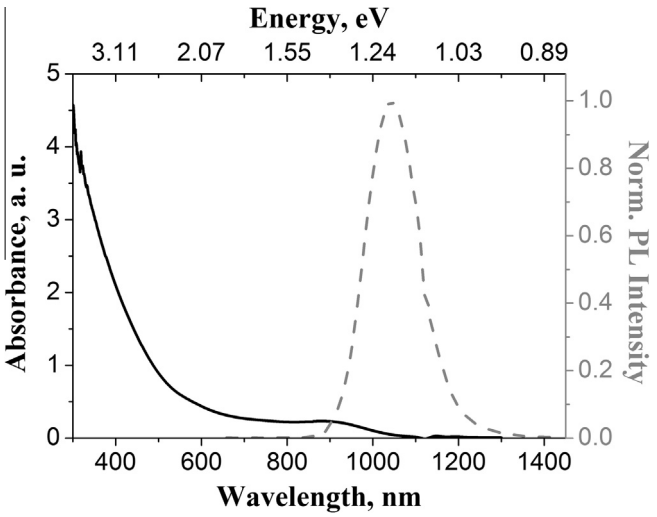

Figure 1. Optical Characterization. Absorbance (solid line) and PL (dash line) spectra for the sample of $Cd_xHg_{(1-x)}Te$ alloy QDs.

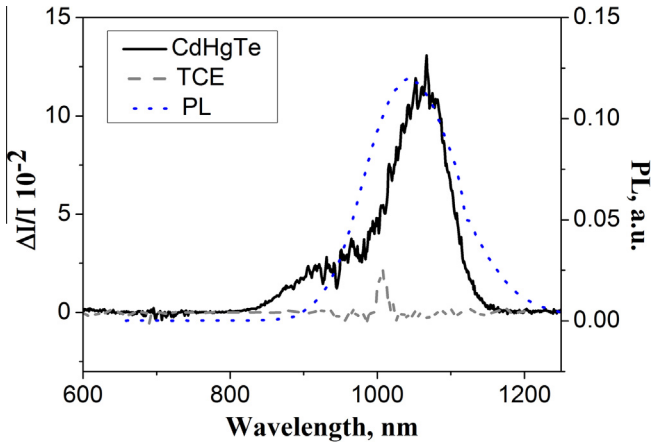

Figure 2. Pump-induced intensity change, $\Delta I/I$ spectra taken for $Cd_xHg_{(1-x)}Te$ alloy QDs (solid line) and TCE (dash line). Pumping was at a wavelength of 500 nm with a spot size of 4 mm and a fluence of 16 μJ/cm^2. Also shown for comparison is the PL intensity (dotted line).2

undergoing second-order diffraction from the grating therein. The first peak in the QD spectrum is at the same spectral position as the absorption edge, and is attributed solely to the bleach caused by state-filling by photo-generated charges, whilst the second is at the position that corresponds to the PL peak shown in Fig. 1 (and reproduced in Fig. 2 to allow direct comparison) and will have contributions from both bleaching and emissive processes. Direct surface-trapping of photogenerated charges has been shown to result in characteristic photo-induced absorption (PIA) features in the vicinity of the band-edge [14,25,26]. However, the pump-induced intensity change spectrum shown in Fig. 2 shows no signs of any such PIA consistent with no significant surface-trapping occurring on this time-scale. The first peak lies outside the PL band and so does not correspond to a transition involving both the valence band maximum (VBM) and the conductance band minimum (CBM) simultaneously. Rather, it must correspond to transitions involving either the VBM or the CBM and another state, with the bleach produced by state-filling of whichever of the band edge states is involved. Similar behaviour has been reported previously for HgTe QDs, and was supported by detailed electronic structure calculations [21]. In contrast the PL band corresponds to a CBM to VBM transition, and here both PL and emission stimulated by the probe beam, as well as bleaching, can result in an increased intensity at the detector. However, the PL intensity is independent of the time-delay between the pump and probe pulses and so appears as a constant background in intensity change transients. Figure S2a in the SI compares transients obtained for probe wavelengths of 920 nm and 1064 nm i.e. outside and within the PL band. A significant background is observed for the latter but none for the former, confirming this interpretation. Thus, in order to simplify the analysis, a probe wavelength of 920 nm was used for the studies described from hereon since that yields an absorption bleach only, and allows the pump-induced response of the CQDs to be expressed in terms of the fractional change in transmittance produced by the bleach.

3.2. Ultrafast exciton dynamics

The quantum yield, *QY*, of MEG can be determined by studying how the dynamics of the bleach peak depend on pump photon energy, $h\nu_p$. The onset of MEG occurs at a threshold value of $h\nu_{p,th}$ that is determined by both the size-dependent band gap, E_g, and the ratio of the effective masses of the electron and hole, m_e^{eff}/m_h^{eff} [27]:

$$h\nu_{p,th} = E_g(2 + m_e^{eff}/m_h^{eff}) \quad (1)$$

For CdHgTe, $m_e^{eff}/m_h^{eff} \approx 0.13$ [28], and thus the MEG threshold occurs at $h\nu_{p,th} \approx 2.1E_g$. Taking the PL peak as a measure of E_g, this relation yields $h\nu_{p,th} = 2.5$ eV for the samples studied, which corresponds to a pump wavelength of ~500 nm. The MEG process can result in more than one additional exciton but this would only occur for an additional increase $h\nu_p$ above E_g of at least the same size [20], i.e. a value of at least $3.2E_g$ for CdHgTe QDs. However, the largest $h\nu_p$ value used in this study is equivalent to $2.8E_g$, and so under these conditions MEG can create only one extra exciton, forming a biexciton.

Biexcitons are also formed when a QD absorbs two photons per pump pulse, the probability of which is determined by the pump fluence and the absorption cross-section at the pump wavelength [29]. Recent work has shown that surface states can trap hot carriers significantly, so that absorbed photons produce band edge excitons with a sample-specific efficiency [30]. However, it is not necessary to know this efficiency, since the band edge occupation, *F*, can be determined directly from the peak fractional transmittance change observed, $\Delta T/T|_{pk}$,, using the following expression [20]:

$$\left.\frac{\Delta T}{T}\right|_{pk} = \frac{A_{pr}}{A}F(1 - e^{-A}) \quad (2)$$

where A_{pr} and A are the sample absorbance at the probe and the pump wavelengths, respectively. Thus *F* is used as a measure of band edge excitation in this study.

Regardless of how they are produced, biexcitons decay into single excitons with a lifetime that is typically several tens of picoseconds; for instance, the lifetime reported for HgTe QDs was 49 ± 2 ps [16]. This is observed in transient absorption data as a sub-nanosecond decay of the bleach feature from its peak value, which is due to state-filling by both biexcitons and single excitons, to a smaller value corresponding to state-filling just by the single excitons that remain. Single excitons have a much longer lifetime, typically several nanoseconds or more, and so the bleach component due to single excitons is observed on the time-scale of the experiment as a constant or a nearly constant plateau [20]. The ratio of the peak to the plateau bleach value, *R*, is given by [27]:

$$R = \delta QY\langle N\rangle[1 - \exp(-\langle N\rangle)]^{-1} \quad (3)$$

where *QY* corresponds to the average number of excitons generated per absorbed photon, $\langle N\rangle$ is the number of photons absorbed per QD per pump pulse and is proportional to *F*, and δ is a factor that takes into account the decay of the single exciton over the duration of the transient. At sufficiently low pump fluences, where $\langle N\rangle$ is negligible, $R/\delta \approx QY$, which will be greater than unity if MEG is significant.

Figure 3 shows the transmittance transients, $\Delta T(t)/T$ for the CdHgTe QDs induced by pumping at a wavelength of 400 nm and at range of excitation levels. The maximum value of the pump-induced bleach varies linearly with pump fluence, as shown in the SI (see Fig. S2b). The decay from this bleach peak is well-described by a mono-exponential decay for $F = 1.2$, 3.1 and 6.9%, and a global fit to these transients yields a time constant of $\tau_B = 91 \pm 1$ ps. Similar decay components have been reported previously for other QDs and attributed to the accumulation of charges trapped on the surface [31–33]. Such surface trapped charges leads to the formation of trions an electron–hole pair is photo-generated whilst the geminate partner of the trapped charge remains in the QD [34]. However, this effect is ameliorated by rapidly stirring or flowing the sample and using only moderate pump fluences. A comparison of the transients obtained for stirred and static samples of the CdHgTe QDs for moderate pump fluence is shown in the SI (see Fig. S3). No significant difference is evident between

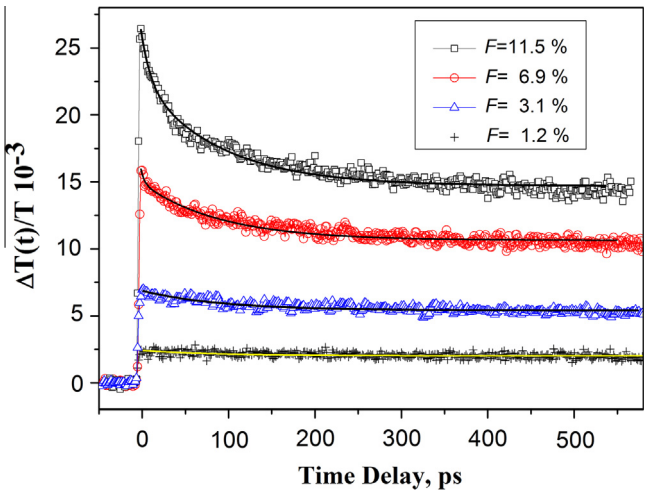

Figure 3. Transmittance transients at a probe wavelength of 920 nm for the $Cd_xHg_{(1-x)}Te$ alloy QDs induced by pumping at a wavelength of 400 nm and various band edge excitation levels, *F*, as shown in the legend. Each of the transients shown is the average of 10 scans and the delay line step size was 0.2 mm. Also shown are mono-exponential fits to the data for $F = 1.2\%$, 3.1% and 6.9% and a bi-exponential fit for $F = 11.5\%$.

the transients, and hence we conclude that the observed sub-nanosecond decay from the peak bleach is not due to the trion recombination that results from the accumulation of trapped charges. As noted above, the absence of any PIA features in the transmittance change spectrum is consistent with no significant charge trapping on a sub-nanosecond time-scale, and we thus conclude the decay with a characteristic lifetime of 91 ps is due to biexciton recombination.

For the maximum excitation level, $F = 11.5\%$, an additional fast component appears at the beginning of decay. This transient is well-described a bi-exponential decay function with a long time constant equal to τ_B and a short time constant of 11 ± 1 ps, which is attributed to the decay of triexcitons. A pump fluence that is sufficiently high to create a substantial population of biexcitons will necessarily produce a significant number of triexcitons as well [29]. Triexciton decay is not normally observed in transient absorption studies because of the twofold degeneracy of the *s*-like CBM commonly found in QDs [35]. State-filling of the CBM by photo-generated electrons is responsible for the pump-induced bleach observed for these QD for a probe wavelength tuned to the absorption edge [35]. The decay of a triexciton into a biexciton does not change the population of such a *s*-like CBM, since it is saturated by the presence of either, and hence the transmission of a probe beam tuned to the absorption edge is not affected. (QDs based on lead chalcogenides are a notable exception to this rule since they have an 8-fold degenerate CBM [36]. However, in this case, the beam used to probe the CdHgTe QDs is tuned to absorption shoulder and not the absorption edge. As discussed in Section 3.1, if CdHgTe QDs have a similar electronic structure to that calculated for HgTe QDs [21], which the similarity of the absorbance and PL spectra between the two types of QDs indicates that they do, then the absorption shoulder will have a significant contribution from the VBM to CBM-1 transition. For HgTe QDs, the VBM is *p*-like [37] and so will have a degeneracy greater than two, and hence will not be completely filled by a biexciton. Unlike in many other types of QD, triexciton decays will thus be observable in our samples of CdHgTe QDs when pumped at sufficiently high fluence.

Transmittance transients were also obtained for pumping at wavelengths of 370 nm, and 750 nm, corresponding to band gap multiples of $2.8E_g$, and $1.4E_g$ and can be found in the SI (see Fig. S4). Figure 4 compares example transients for each of the pump wavelengths used – further transients acquired for a range excitation levels are given in the SI. As shown in Fig. 4, the decays from the bleach peak resulting from pumping at each of these wavelengths can all be well-described by a mono-exponential function with a 91 ps lifetime, showing that the sub-nanosecond dynamics observed both above and below the threshold for MEG are consistent with biexciton formation and recombination.

Confirming that the observed dynamics are free of trapping effects in this way enables Eq. (2) to be used to determine the *QY* of MEG. Figure 5 shows the values of *R* determined for pump wavelengths below and above the MEG threshold as a function of excitation level, *F*. Also shown in Fig. 5 are fits of Eq. (3) to the data. The value of δ used for the fits was calculated from

$$\delta = exp\left(\frac{t_{plateau} - t_{peak}}{\tau_{PL}}\right)^{\beta} \quad (4)$$

where $(t_{plateau} - t_{peak})$ is the period between the peak bleach and a time by which biexciton recombination is complete and the bleach transient has reached a constant plateau, which in this study was chosen to be $5\tau_B \approx 0.5$ ns; τ_{PL} and β are the lifetime and stretching exponent, respectively, that characterize the PL decay. The PL transient obtained for this sample has been previously reported [9] to be $\tau_{PL} = 64.9 \pm 0.6$ ns and $\beta = 0.80 \pm 0.01$, which gives $\delta = 1.021 \pm 0.001$. Using this value resulted in the fits shown and yielded $QY = 1.01 \pm 0.01$, 1.15 ± 0.01 and 1.05 ± 0.02 for $h\nu_p = 1.4E_g$, $2.6E_g$, and $2.8E_g$, respectively. The uncertainty in these *QY* values comes predominantly from the fits to the data shown in Figs. 5 and S5, the contribution from the uncertainty in δ being negligible. The first of these *QY* values is not significantly different from unity, as expected for pumping below the MEG threshold. In contrast, the other two pump photon energies are greater than $h\nu_{p,th}$ and consequently yield a *QY* increased by MEG.

The highest *QY* value obtained here was that of 1.15 ± 0.01 when photo-exciting with $h\nu_p = 2.6E_g$. In contrast, a quantum yield of 1.39 ± 0.13 was recently reported for CdHgTe QDs [9] when photo-exciting with $h\nu_p = 4.28$ eV, which was described as corresponding to $3E_g$. However, the authors used the position of the absorption shoulder as a measure of the E_g rather than that of the PL peak, as in this study. As shown in Fig. 1, there is a large

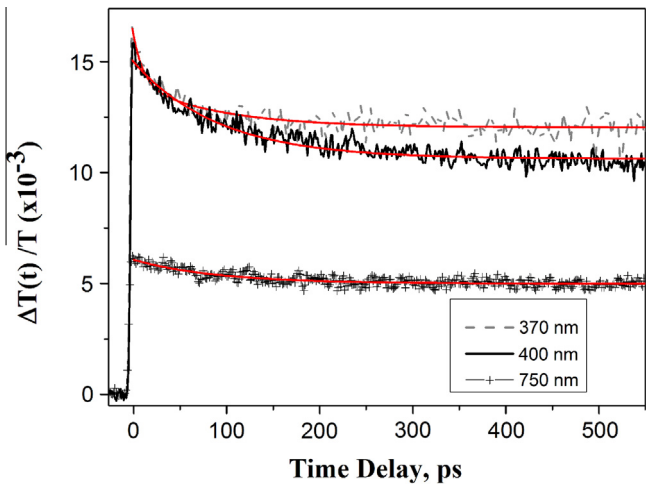

Figure 4. Comparison of transmittance change transients produced by excitation wavelengths of 370 nm (dash line), 400 nm (solid line), and 750 nm (crosses); the band edge excitation levels were that of $F = 6.7\%$, 6.9% and 5.1% respectively. In each case, the probe beam wavelength was set to 920 nm, the position of the bleach peak. Each trace is the average of 10 scans with a delay line step size of 0.2 mm. Also shown are mono-exponential fits to the 400 nm and 750 nm decays yielding a time constant of 91 ps, and a bi-exponential fit to the 370 nm decay, with time constants of 11 ps and 91 ps.

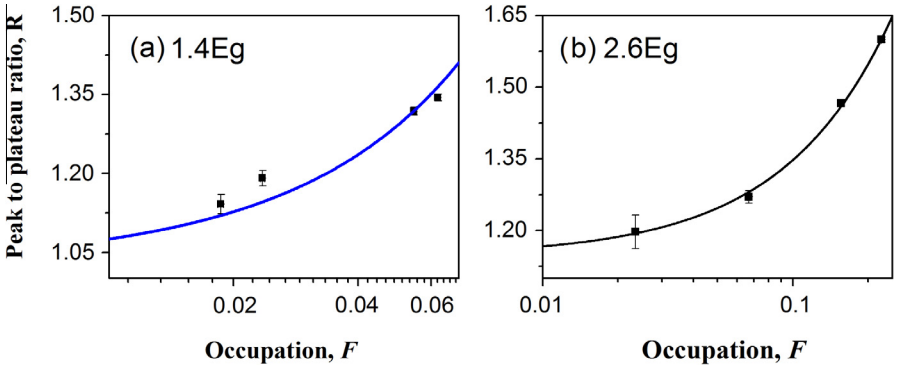

Figure 5. Peak to plateau ratio, R, of the transmittance transients induced by a pump beam of wavelengths of (a) 1.4 times and (b) 2.6 times the band edge for $Cd_xHg_{(1-x)}Te$ alloy QDs as a function of F; the fit shown is to Eq. (3)). See also Figure S4 in SI the $2.8E_g$ case.

difference in spectral position between the PL peak and the absorption shoulder, and so the two different approaches result in significantly different values of E_g. Moreover, as discussed in Section 3.1, electronic structures for HgTe QDs indicate that absorption shoulder does not correspond to the VBM to CBM transition and thus is not equivalent to E_g. Using instead the position of the PL peak described in Ref. [9], for a better comparison with this work, yields $E_g = 1.24$ eV, so that $h\nu_p = 4.28$ eV now corresponds to $3.5E_g$. An increase from $QY = 1.15 \pm 0.01$ to 1.39 ± 0.13 as $h\nu_p$ rises from $2.6E_g$ to $3.5E_g$is similar to the increase predicted for HgTe QDs over the same range using a tight-binding model of MEG [21], suggesting that the QY values reported in Ref. [9] and here are consistent. The same model also predicts that QY does not monotonically rise with increasing $h\nu_p$, but rather that there are several peaks in QY, particularly as $h\nu_p$ grows from $\sim 2E_g$ to $3.5E_g$. This is similar to the drop in QY observed here for CdHgTe QDs as $h\nu_p$ rises from $2.6E_g$ and $2.8E_g$. Similar behaviour has been also reported previously in a detailed theoretical study of MEG in α-Sn QDs based on the same tight-binding model [38]. That work attributed the peaks found in the calculated MEG QY as $h\nu_p$ varied to optical transitions within the near-band edge electronic structure with particularly high rates of MEG.

The MEG QY for other types of QDs with an absorption edge similarly well-suited to the solar spectrum have also been reported. The MEG thresholds for isolated PbSe [32,39] and PbS [23] QDs have been reported to be significantly greater, at $\sim 3E_g$, than the minimum of $2E_g$ required by energy conservation [12], so no significant MEG would occur at the values of $h\nu_p$ used here or Ref.[9]. However, the threshold for PbSe QDs reduces to $h\nu_{p,th} \approx 2E_g$ when the QDs are deposited as a film and at $h\nu_p = 3E_g$ the QY rises to 1.4 [40]. In contrast, for InAs QDs $h\nu_{p,th} \approx 2E_g$ and at $h\nu_p = 3E_g$ $QY = 1.35$ [41]. Ge [42] and Si [43] QDs both have $h\nu_{p,th} \approx 2E_g$ and $QY = 2.0$ at $h\nu_p = 3E_g$. However, these QDs were formed in a silica matrix and so are not solution processable like colloidal QDs. Thus, the CdHgTe QDs studied here combine a solar-suitable band gap and competitive MEG efficiency with solution-phase processing.

The rise of the bleach signal corresponds to the cooling of hot excitons to the band edge, and is shown in Fig. 6 for $h\nu_p = 1.4E_g$, $2.6E_g$ and $2.8E_g$. The time taken for the signal to rise from zero to its maximum value was measured to be 1.1 ± 0.1 ps, 4.1 ± 0.1 ps and 5.1 ± 0.2 ps for these pump photon energies, respectively. An energy of $h\nu_p - E_g$ is lost by each initially photogenerated hot exciton during this process and so these cooling times correspond to a rate of energy of loss of 0.43 ± 0.04 eV ps^{-1}, 0.46 ± 0.01 eV ps^{-1}, and 0.42 ± 2 eV ps^{-1}, respectively. MEG is an additional process by which the hot exciton loses energy and so would be expected to increase the rate of energy loss. The highest rate is observed for the value of $h\nu_p$ corresponding to the highest QY, although the

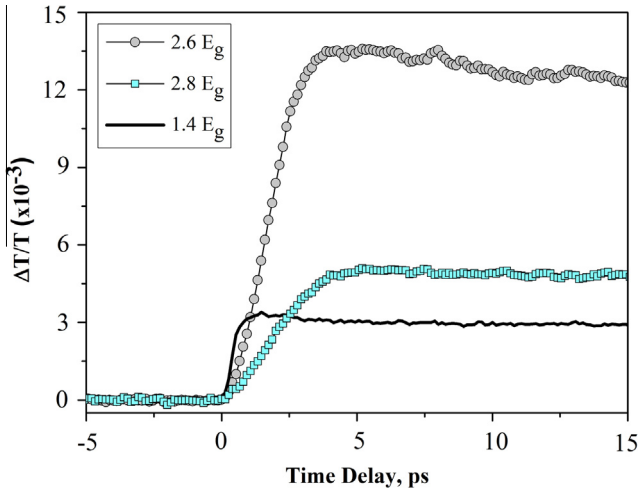

Figure 6. Initial bleach rise times for $Cd_xHg_{(1-x)}Te$ alloy QDs when pumped with $h\nu_p$ above (circles and squares) and below (solid line) the MEG threshold. Each of the transients shown is the average of 10 scans and the delay line step size was 0.02 mm.

increase in rate is similar in size to the accuracy of the measurement. Nevertheless, this observation is consistent with an increased rate of MEG increasing both the QY and the overall cooling rate.

4. Summary and conclusions

Ultrafast transient absorption spectroscopy has been used to investigate the exciton dynamics in $Cd_xHg_{(1-x)}Te$ alloy QDs. At modest pump fluences, the sample was found to be free of the effects of surface trapping. Hence the transient decays obtained below the MEG threshold where attributed to biexciton recombination created by two photons, while in the above MEG threshold case the decay of the transients is attributed to bi-exciton recombination due to both the absorption of two photons and MEG. A contribution due to triexciton formation at higher pump fluences was also observed. The QY of MEG was found to be 1.15 ± 0.01 when the sample was photo-excited with a photon energy 2.6 times the band gap; this result found to be consistent with a previous study based on an alternative technique.

Author contributions

MAL and AlO performed the experiments and analyzed the data; SVK, ALR, OZ and SK provided the materials; SM and DM provided the TEM image; MAL and DJB wrote the paper.

Conflicts of Interest

The authors declare no conflict of interest.

Acknowledgments

MAL and DJB acknowledge EPSRC for financial support (Grant number EP/K008544/1). AAl-O thanks the Ministry of Higher Education of Saudi Arabia for the financial support. SVK and ALR thank the Research Grants Council of Hong Kong S.A.R. for financial support (GRF project 102412). The authors would like to thank Lazo Kakou for the graphical abstract.

Appendix A. Supplementary data

Supplementary data associated with this article can be found, in the online version, at http://dx.doi.org/10.1016/j.chemphys.2016.02.003.

The experimental data from this study are available at http://dx.doi.org/10.15127/1.296944.

References

[1] I.J. Kramer, E.H. Sargent, ACS Nano 5 (2011) 8506.
[2] W.J. Cai, L.M. Jiang, D.M. Yi, H.Z. Sun, H.T. Wei, H. Zhang, H.C. Sun, B. Yang, Langmuir 29 (2013) 4119.
[3] D.V. Talapin, J.S. Lee, M.V. Kovalenko, E.V. Shevchenko, Chem. Rev. 110 (2010) 389.
[4] Y. Shirasaki, G.J. Supran, M.G. Bawendi, V. Bulovic, Nat. Photonics 7 (2013) 13.
[5] F. Aslam, J. Stevenson-Hill, D.J. Binks, S. Daniels, N.L. Pickett, P. O'Brien, Chem. Phys. 334 (2007) 45.
[6] M.C. Hanna, A.J. Nozik, J. Appl. Phys. 100 (2006).
[7] S.H. Im, H.J. Kim, S.W. Kim, S.W. Kim, S.I. Seok, Nanoscale 4 (2012) 1581.
[8] S. Gupta, O. Zhovtiuk, A. Vaneski, Y.C. Lin, W.C. Chou, S.V. Kershaw, A.L. Rogach, Part. Part. Syst. Char. 30 (2013) 346.
[9] S.V. Kershaw, S. Kalytchuk, O. Zhovtiuk, Q. Shen, T. Oshima, W. Yindeesuk, T. Toyoda, A.L. Rogach, Phys. Chem. Chem. Phys. 16 (2014) 25710.
[10] R.D. Schaller, V.I. Klimov, Phys. Rev. Lett. 92 (2004) 186601.
[11] V.I. Rupasov, V.I. Klimov, Phys. Rev. B 76 (2007).
[12] C. Smith, D. Binks, Nanomater.-Basel 4 (2014) 19.
[13] S. ten Cate, C.S.S. Sandeep, Y. Liu, M. Law, S. Kinge, A.J. Houtepen, J.M. Schins, L. D.A. Siebbeles, Accounts Chem. Res. 48 (2015) 174.
[14] P. Tyagi, P. Kambhampati, J. Chem. Phys. 134 (2011).
[15] M. Cadirci, S.K. Stubbs, S.J.O. Hardman, O. Masala, G. Allan, C. Delerue, N. Pickett, D.J. Binks, Phys. Chem. Chem. Phys. 14 (2012) 15166.
[16] M. Cadirci, S.K. Stubbs, S.M. Fairclough, E.J. Tyrrell, A.A.R. Watt, J.M. Smith, D.J. Binks, Phys. Chem. Chem. Phys. 14 (2012) 13638.
[17] P. Kambhampati, J. Phys. Chem. C 115 (2011) 22089.
[18] S.K. Stubbs, S.J.O. Hardman, D.M. Graham, B.F. Spencer, W.R. Flavell, P. Glarvey, O. Masala, N.L. Pickett, D.J. Binks, Phys. Rev. B 81 (2010).
[19] A. Rogalski, Rep. Prog. Phys. 68 (2005) 2267.
[20] D.J. Binks, Phys. Chem. Chem. Phys. 13 (2011) 12693.
[21] A. Al-Otaify, S.V. Kershaw, S. Gupta, A.L. Rogach, G. Allan, C. Delerue, D.J. Binks, Phys. Chem. Chem. Phys. 15 (2013) 16864.
[22] S.L. Wu, J. Dou, J. Zhang, S.F. Zhang, J. Mater. Chem. 22 (2012) 14573.
[23] S.J.O. Hardman, D.M. Graham, S.K. Stubbs, B.F. Spencer, E.A. Seddon, H.T. Fung, S. Gardonio, F. Sirotti, M.G. Silly, J. Akhtar, P. O'Brien, D.J. Binks, W.R. Flavell, Phys. Chem. Chem. Phys. 13 (2011) 20275.
[24] A. Al-Otaify, M.A. Leontiadou, F.V.E. dos Reis, T.C. Damato, P.H.C. Camargo, D.J. Binks, Phys. Chem. Chem. Phys. 16 (2014) 14189.
[25] H.M. Zhu, Y. Yang, K. Hyeon-Deuk, M. Califano, N.H. Song, Y.W. Wang, W.Q. Zhang, O.V. Prezhdo, T.Q. Lian, Nano Lett. 14 (2014) 1263.
[26] M. Califano, ACS Nano 9 (2015) 2960.
[27] M.C. Beard, R.J. Ellingson, Laser Photonics Rev. 2 (2008) 377.
[28] A. Bouazzi, Y. Marfaing, J. Mimilaarroyo, Rev. Phys. Appl. 13 (1978) 145.
[29] V.I. Klimov, Annu. Rev. Phys. Chem. 58 (2007) 635.
[30] C.T. Smith, M.A. Leontiadou, R. Page, P. O'Brien, D.J. Binks, Adv. Sci. (2015) 1500088.
[31] J.A. Mcguire, J. Joo, J.M. Pietryga, R.D. Schaller, V.I. Klimov, Accounts Chem. Res. 41 (2008) 1810.
[32] A.G. Midgett, H.W. Hillhouse, B.K. Hughes, A.J. Nozik, M.C. Beard, J. Phys. Chem. C 114 (2010) 17486.
[33] J.A. McGuire, M. Sykora, J. Joo, J.M. Pietryga, V.I. Klimov, Nano Lett. 10 (2010) 2049.
[34] M. Califano, F.M. Gomez-Campos, Nano Lett. 13 (2013) 2047.
[35] V.I. Klimov, J. Phys. Chem. B 104 (2000) 6112.
[36] I. Kang, F.W. Wise, J. Opt. Soc. Am. B 14 (1997) 1632.
[37] G. Allan, C. Delerue, Phys. Rev. B 86 (2012).
[38] G. Allan, C. Delerue, ACS Nano 5 (2011) 7318.
[39] N.J.L.K. Davis, M.L. Bohm, M. Tabachnyk, F. Wisnivesky-Rocca-Rivarola, T.C. Jellicoe, C. Ducati, B. Ehrler, N.C. Greenham, Nat. Commun. 6 (2015).
[40] C.S.S. Sandeep, S. Ten Cate, J.M. Schins, T.J. Savenije, Y. Liu, M. Law, S. Kinge, A.J. Houtepen, L.D.A. Siebbeles, Nat. Commun. 4 (2013).
[41] R.D. Schaller, J.M. Pietryga, V.I. Klimov, Nano Lett. 7 (2007) 3469.
[42] S. Saeed, C. de Weerd, P. Stallinga, F.C.M. Spoor, A.J. Houtepen, L.D.A. Siebbeles, T. Gregorkiewicz, Light-Sci. Appl. 4 (2015).
[43] M.T. Trinh, R. Limpens, W.D.A.M. de Boer, J.M. Schins, L.D.A. Siebbeles, T. Gregorkiewicz, Nat. Photonics 6 (2012) 316.